Received January 3, 2020, accepted January 13, 2020, date of publication January 20, 2020, date of current version January 30, 2020.
Digital Object Identifier 10.1109/ACCESS.2020.2968187

A 3-D Printed Spherical Antenna With Bandwidth Enhancement Under Operation of Dual Resonance

YU-JIAN ZHU[1], JIN LI[1,2], (Member, IEEE), XIAO ZHANG[1], (Member, IEEE), TAO YUAN[1,3], (Member, IEEE), ZENG-PEI ZHONG[1], TING-YAN TAN[1], AND XIAO-KUN BI[1]
[1]Guangdong Provincial Mobile Terminal Microwave and Millimeter-Wave Antenna Engineering Research Center, College of Electronics and Information Engineering, Shenzhen University, Shenzhen 518060, China
[2]State Key Laboratory of Millimeter Waves, Nanjing 210096, China
[3]ATR National Key Laboratory of Defense Technology, College of Electronics and Information Engineering, Shenzhen University, Shenzhen 518060, China
Corresponding author: Xiao-Kun Bi (gsh870512@163.com)

This work was supported in part by the National Natural Science Foundation of China under Grant 61801298, in part by the State Key Laboratory of Millimeter Waves under Grant K202036, in part by the Fundamental Research Program of Shenzhen Science and Technology Innovation Committee, China, under Project JCYJ20180305124721920, and in part by the Shenzhen Innovation and Entrepreneurship Program for Overseas High-Level Talents, China, under Project KQTD20180412181337494.

ABSTRACT In this paper, a three-dimensional (3-D) printed spherical antenna with bandwidth enhancement under the operation of TM_{101} and TM_{211} modes is presented. The antenna is started from a metallized spherical cavity with a rectangular feed waveguide. Then, some slots are suitably introduced on its sidewall. With the help of these introduced slots, two resonant modes (TM_{101} and TM_{211}) can be excited simultaneously and merged with each other, resulting in a wideband radiation characteristic with two resonances. An antenna prototype operating at *X* and *Ku* bands is designed and implemented as proof of concept. The antenna is additively manufactured by incorporating polymer-based stereolithography and electroless copper plating techniques. Measured results show that the antenna not only owns a wide impedance bandwidth of 40.9% from 9.77 to 14.81 GHz, but also maintains stable radiation patterns over the operating band. Besides, the measured average gain is as high as 10.1 dBi. As the measured results are in good agreement with the simulated ones, a simple and effective design of 3-D printed wideband spherical antenna with high radiation performances is verified.

INDEX TERMS Spherical antenna, 3-D printed, waveguide-fed, wideband antenna.

I. INTRODUCTION

Due to the desirable advantages, such as high radiation gain, low loss, high power handling capacity, and simple feeding, waveguide slot antennas have been widely used in modern telecommunication systems [1]. Various slot antennas based on annular [2], cylindrical [3], and rectangular waveguides [4] have been reported in open literature. However, such reported antennas suffer from intrinsically narrow operation bandwidth duo to only a single radiation mode excited and employed, which will restrict their applications in the high data-rate wireless communication systems.

Two methods have been reported to date to improve bandwidth of the waveguide slot antennas. The first one is to use rectangular ridge waveguide [5], [6]. By separating the array into two subarrays, the antennas' impedance bandwidth can be broaden. The second one is to use multilayer and corporate-fed structure [7]–[9]. It was realized with the help of diffusion bonding of laminate thin metal plates. Unfortunately, the slot antennas based on these two methods are not only difficult and expensive to fabricate, but also own limited impedance bandwidth from 7.8% to 30%.

To further increase the bandwidth, one of the alterative methods is to merge some radiation modes together, which has been extensively studied in patch antennas [10]–[12]. However, few literatures have suggested this method to increase the bandwidth of the waveguide slot antennas. The reason is that the cross polarization and radiation patterns of the antenna will be deteriorated significantly when the extra slots are introduced on the waveguide for exciting high-order modes.

The associate editor coordinating the review of this manuscript and approving it for publication was Mengmeng Li.

It is known from [13] that there are diverse resonant modes exist in a metal spherical resonator. It is promising to realize a spherical cavity based wideband antenna by merging some radiation modes together without degrading radiation performance. Pioneering studies on theory and analytical calculation of the radiation performance for slotted spherical cavities have been presented in [14]–[18]. However, few practical slotted spherical antennas have been demonstrated. One of the important reasons is that the fabrication of these derives through conventional manufacturing technology is a great challenge.

With the rapid development of three-dimensional (3-D) printing technology, an alternative solution for the implementation of microwave antennas has been provided [19], [20]. It presents many attractive advantages over the traditional subtractive manufacturing techniques, such as, higher manufacturing accuracy and efficiency, lower cost, and more flexibility in structural design. By 3-D printing, monolithically manufacturing of the devices can be achieved, and the performance degradation due to assembly can be avoided.

As one of the 3-D printing techniques, stereolithography apparatus (SLA) features a high printing resolution and a small surface roughness, which has been widely utilized to fabricate high performance microwave devices, such as, slotted waveguide array [21] and spherical resonator based waveguide filters [22], [23]. These devices are initially formed by curing photosensitive resin layer by layer, and then surface-metallized with high conductive metal, such as, copper. Therefore, it is feasible to fabricate a practical spherical-cavity-based slot antenna component by 3-D printing.

In this paper, a 3-D printed spherical antenna under the operation of TM_{101} and TM_{211} resonant modes is proposed toward its bandwidth enhancement under dual resonance. By symmetrically and suitably cutting five circumferential slots on the shell of a metallized spherical resonator, two resonant modes TM_{101} and TM_{211} can be excited simultaneously and merged with each other, resulting in a wideband characteristic with two resonances. A prototype is fabricated monolithically by incorporating SLA and electroless copper plating techniques. Measured results show that the antenna not only provides a wide fractional bandwidth (FBW) of 40.9% from 9.77 to 14.81 GHz, but also maintains stable radiation patterns over the operating band. Furthermore, due to the use of low-density resin as the building material, the weight of the antenna is dramatically reduced compared to the conventional metal ones. To the best knowledge of authors, the slot-loaded wideband spherical antenna designed by merging two radiation modes together have not been reported.

II. DESIGN OF THE SLOTTED SPHERICAL ANTENNA

A. ANTENNA GEOMETRY

Fig. 1 depicts the geometry of the proposed slot-loaded spherical antenna. Seen from it, the proposed antenna, which is fed by a rectangular waveguide through a coupling window, is mainly constructed by a metallized spherical resonator with

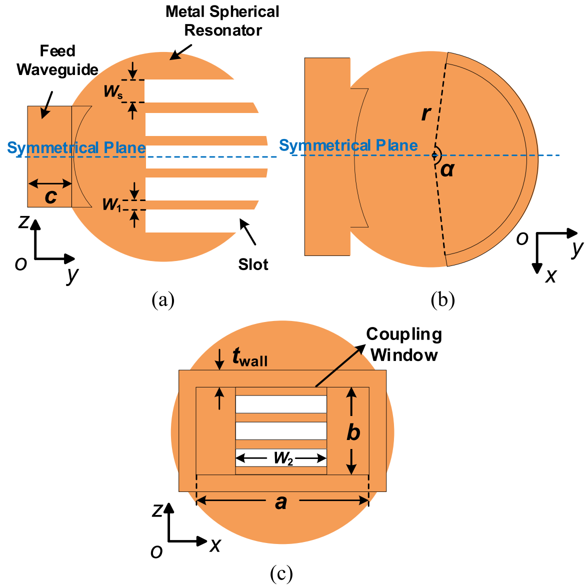

FIGURE 1. Simplified geometrical illustrations of the proposed slotted spherical antenna. The waveguide flange is excluded in the illustrations. (a) The *yoz* -plane view. (b) The *xoy* -plane view. (c).The *xoz*-plane view.

five circumferential slots. The slot size is determined by the width W_S and angle α, and the spacing between adjacent slots is W_1. The length of the feed waveguide is c, and the size of the coupling window is $b \times W_2$. t_{wall} is the shell thickness of the antenna. Since the antenna is designed to operate at X and Ku bands, the model of the feed waveguide is correspondingly selected as WR-90. The parameters of a and b represent the lengths of the waveguide broad and narrow walls, respectively.

B. RESONANT MODES

To better understand the working mechanism of the antenna, the resonant modes in an air-filed metal spherical cavity are analyzed. The fundamental mode and first spurious mode of the spherical resonator are TM_{101} and TM_{211}, respectively [13]. The eigenmode frequencies of these two modes are mainly determined by inner radius of the spherical resonator, and their values can be calculated by using the equations (1) and (2)

$$f_{TM101} = \frac{\omega_{TM101}}{2\pi} = \frac{y_{11}}{2\pi r\sqrt{\mu\varepsilon}}, \quad (1)$$

$$f_{TM211} = \frac{\omega_{TM211}}{2\pi} = \frac{y_{21}}{2\pi r\sqrt{\mu\varepsilon}}, \quad (2)$$

where ω_{TM101} and ω_{TM211} are the corresponding natural angular frequencies, r is the inner radius of the spherical resonator, y_{11} and y_{21} are the roots of Bessel function. By looking up the mode chart in [13], the values of y_{11} and y_{21} for TM_{101} and TM_{211} modes are found to be 2.744 and 3.870, respectively. The parameters μ and ε are permeability and permittivity of the dielectric filled in the resonator. In free space, the resonant frequency of the two aforementioned

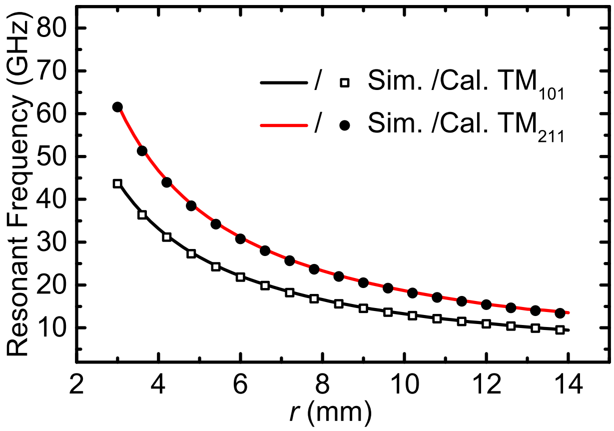

FIGURE 2. Calculated and EM-simulated eigenmode resonant frequencies of the TM_{101} and TM_{211} modes versus the inner radius of the metal spherical cavity resonator.

modes can be simplified as (3) and (4)

$$f_{TM101} \approx 1.3102 \times 10^{11}/r \quad (3)$$
$$f_{TM211} \approx 1.8478 \times 10^{11}/r \quad (4)$$

Here, the unit of f is Hz and r is millimeter. The calculated and EM-simulated eigenmode frequencies of the TM_{101} and TM_{211} modes under different radius r are plotted in Fig. 2. The numerical calculation was carried out in MATLAB [24]. It is obvious that the resonant frequencies for each modes is mainly determined under a specified value r. In this design, the inner radius r is 12.9 mm. Thus, the modes TM_{101} and TM_{211} are operating at *X* and *Ku* bands, respectively.

C. RADIATION PRINCIPLE

Fig. 3 shows the simulated surface current distribution of the TM_{101} and TM_{211} modes on a waveguide-fed metal spherical cavity. The surface current distribution was obtained by using ANSYS high frequency structure simulator (HFSS), version 18.2 [25]. It can be seen from *yoz*-plane in Fig. 3, the current distribution of these two modes has the same direction in the blue dashed area and is almost perpendicular to the *xoy*-plane. Therefore, when some slots are cut on the blue dashed area and along the direction perpendicular to the current line to interrupt the current distribution, these two modes can be radiated simultaneously and a vertical linearly polarized electrical filed can be generated. One thing should be noted that when the slot is cut such that the long dimension runs along the current direction, only a small perturbation to the current distribution is produced, theoretically, little radiation is generated under this case [26]. Besides, if the long dimension of the slot is not perpendicular to the current direction, a horizontally polarized electric field component will be introduced, and thus the cross polarization of the antenna will be deteriorated. So, in order to ensure the cross-polarization as low as possible, all the slots in this design are loaded in an orientation perpendicular to the current directions, as shown in Fig. 1.

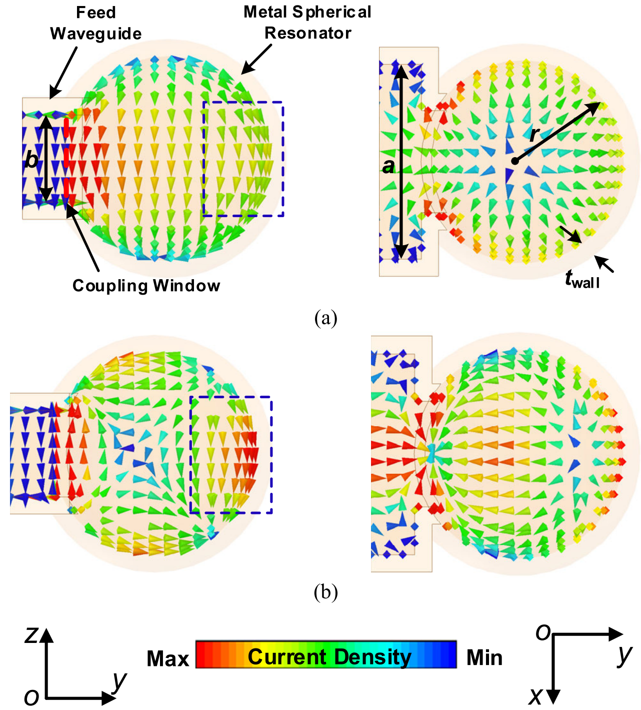

FIGURE 3. Simulated surface current distribution of the TM_{101} and TM $_{211}$ modes in a waveguide-fed spherical cavity resonator with inner radius r = 12.9 mm and shell thickness t_{wall} = 2 mm. (left: *yoz*-plane; right: *xoy* -plane).The waveguide flange is excluded in the illustrations. (a) The TM_{101} mode.(b) The TM $_{211}$ mode.

TABLE 1. Critical parameters of the proposed waveguide-fed slotted spherical antenna.

a (mm)	b (mm)	c (mm)	r (mm)	W_S (mm)	W_1 (mm)	W_2 (mm)	t_{wall} (mm)	φ (°)	N
22.86	10.16	5	12.9	3.5	1	17.8	2	190	5

More importantly, it is found that the resonant frequencies of the TM_{101} and TM_{211} can be merged together by elaborately adjusting the size of the slot and coupling window, so that the bandwidth of antenna can be widened significantly.

D. ANTENNA ANALYSIS AND PARAMETRIC STUDIES

In this paper, when one parameter is studied, the other parameters are fixed as listed in Table. I. The antenna analysis was performed numerically using HFSS. Copper (electrical conductivity of 5.96 × 10^7 S/m) boundary was used in the simulation of this work.

A graphical comparison of the reflection coefficient under different slots number N is illustrated in Fig. 4. Obviously, two resonant modes can be observed in these three cases. The lower resonance frequency relates to TM_{101} mode, while the higher resonance frequency relates to TM_{211} mode. Besides, it can be seen clearly that the reflection coefficient of TM_{211} increases significantly as N increases.

Next, the effect of the slot width on the resonant frequency of TM_{101} and TM_{211} modes is investigated. In Fig. 5, the reflection coefficients of the proposed antenna respect

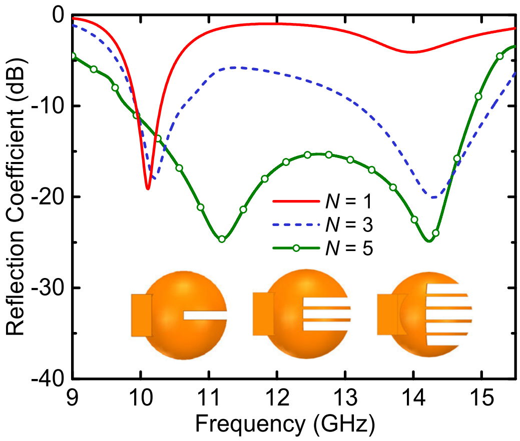

FIGURE 4. Simulated reflection coefficient under different slot numbers ***N***.

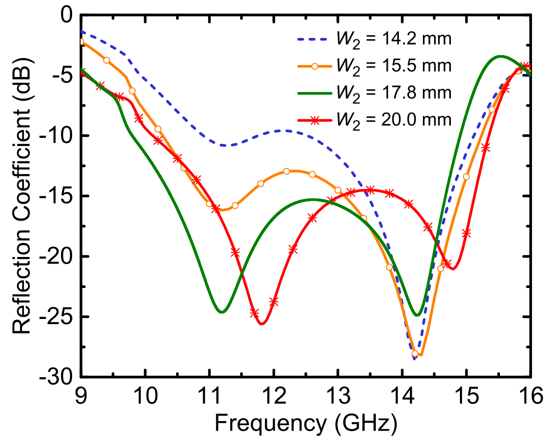

FIGURE 6. Simulated reflection coefficient under different length of coupling window W_2.

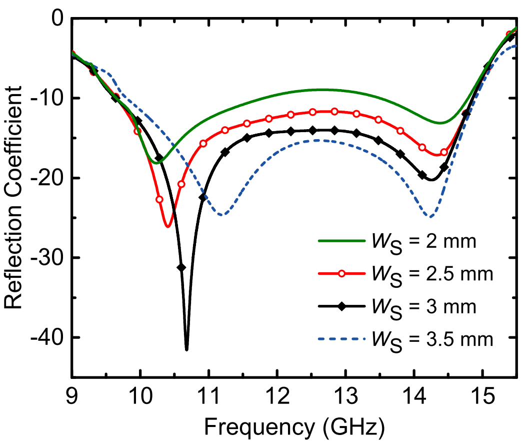

FIGURE 5. Simulated reflection coefficient under different slot width W_S.

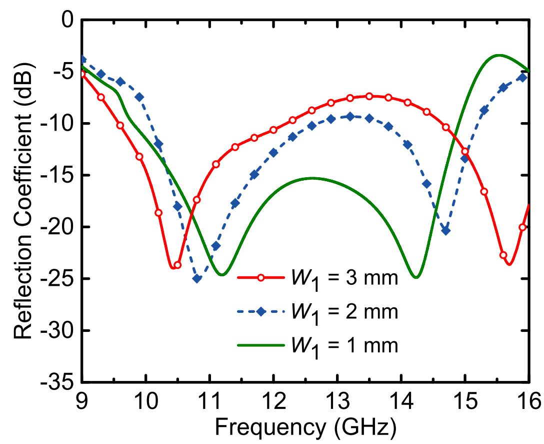

FIGURE 7. Simulated reflection coefficient under different width of adjacent slots W_1.

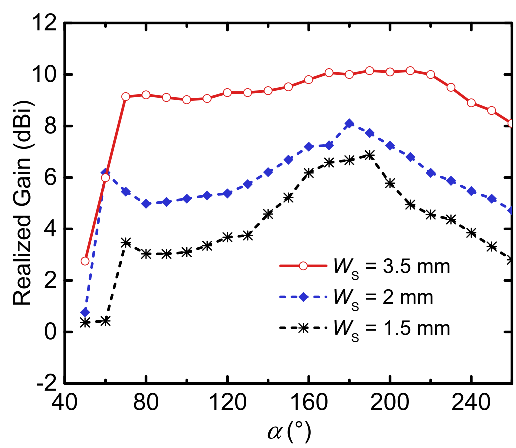

FIGURE 8. Simulated realized gain of the proposed antenna at 11.5 GHz versus the slot angle α under different slot width W_S.

to different slot width W_S are plotted. It can be observed that the resonant frequency of TM_{101} tends to move upwards gradually with the increase of slot width W_S, while the one of TM_{211} is rarely changed. It provides the possibility to merge the resonant frequencies of these two modes by suitably selected the value of W_S.

The reflection coefficient with respect to different length of coupling window W_2 is illustrated in Fig. 6. The results show that the impedance matching of TM_{101} can be improved by adjusting W_2. When W_2 equals to 17.8 mm, the resonant frequencies of TM_{101} and TM_{211} can be well merged, resulting in a wide impedance bandwidth.

Fig. 7 shows the reflection coefficient under different width of adjacent slots W_1. It is observed that changing W_1 has an opposite effect on the resonant frequencies of TM_{101} and TM_{211}. In order to keep the resonant frequencies of these two modes as close as possible, W_1 was set to be 1.0 mm. One thing should be noticed that when W_1 is less than 1.0 mm, the antenna will not be easy to manufacture due to its fragile structure.

The relationships between the realized gain and the slot parameters are also investigated. The simulated realized gain versus the slot angle α under different slot width W_S at 11.5 GHz is depicted in Fig. 8. Seen from it, the realized gain would be increased largely when W_S increases from 1.5 mm to 3.5 mm. However, it has been demonstrated that after W_S

exceeds 3.5 mm, continuing to increase W_S does not increase the realized gain significantly, but weaken the mechanical strength of the antenna. To tradeoff the antenna performances and mechanical strength, W_S is selected as 3.5 mm. The slot angle α is also an important parameter effecting the realized gain of the antenna. It is interesting that the realized gain has a tendency to increase first and then decrease as α increases from 50 to 260 degrees, and reaches the maximum at about $\alpha = 190°$.

The shell thickness of the antenna is t_{wall}. Theoretically, if the inner radius of the spherical resonator is determined, the parameter of t_{wall} has little effect on antenna performance. In this design, t_{wall} was set to be 2.0 mm, whose aim is not only to ensure sufficient mechanical strength, but also to save fabrication costs.

According to the above analysis, the final dimensions of the proposed antenna are determined and the values of all the parameters are listed in Table 1. Fig. 9 shows the simulated 3-D radiation patterns at 10.2 GHz, 11.4 GHz, 12.2 GHz and 14.8 GHz respectively. Apparently, stable directional radiation patterns can be obtained over the entire impedance bandwidth.

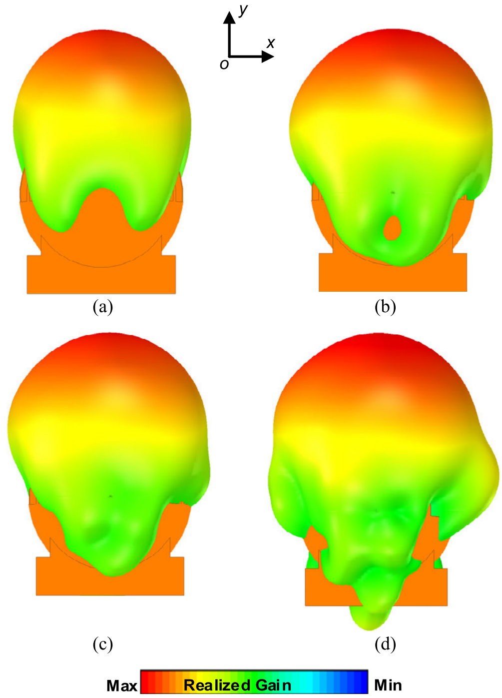

FIGURE 9. Simulated 3-D radiation patterns of the proposed antenna. (a) At 10.2 GHz. (b) At 11.4 GHz. (c) At 12.2 GHz. (d) At 14.8 GHz.

III. ANTENNA FABRICATION

The devised antenna was additively manufactured by incorporating resin-based SLA and electroless copper plating process. Similar manufacturing approaches have been reported in the fabrication of microwave devices [22], [23]. The 3-D printed antenna in this work has the following advantages: 1. The manufacturing efficiency is significantly improved. 2. Errors caused by assembly can be avoided. 3. The weight of the antenna is highly reduced without sacrificing any RF performances.

A. SLA PRINTING

Soildworks [27] can be used to export a stereolithography (STL) format design file, which can be directly used for 3-D printing. The antenna model was placed in an orientation as illustrated in Fig. 10 for the SLA printing. Such an orientation allowed monolithic 3-D printing of the entire antenna structure with minimized use of resin supporting material, and the little resin support was used near the feeding window and at bottom of the waveguide flange. The resin support could be removed easily after the 3-D printing process. The SLA printing was carried out in a vertical printing resolution of 50 μm. The feeding waveguide and its flange were mated to the antenna during printing process, so no further assembly is required after printing. The ceramic-filled photosensitive resin Somos PerForm [28] was used as the printing materials in this design due to high mechanical strength and high thermal handling capability.

B. SURFACE METALLIZATION

After the 3-D printing process was completed, surface metallization process was carried out by electroless plating. In the metallization process, a 10 μm thick conductive layer of copper was plated on the resin model. The thickness of copper is 10× larger than the skin depth (≈0.729 μm) calculated at 8 GHz. The sufficient copper thickness ensures good conductivity and reduces the loss from copper. To minimize the tolerance induced by the plated copper, a structural compensation was performed to the electronic model before the 3-D printing, where a 10-μm thick layer was subtracted. The fabricated antenna prototype before and after copper plating are shown in Fig. 10.

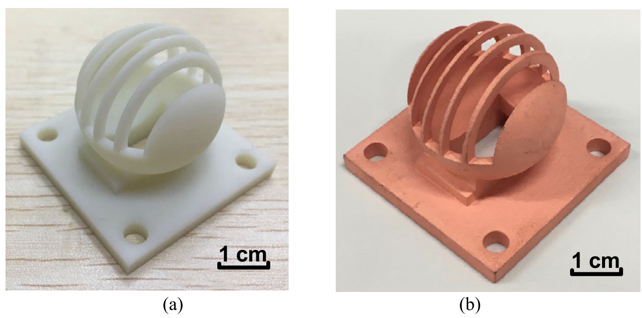

FIGURE 10. Photographs of the antenna before and after plating. (a) Before plating. (b) After plating.

The 3-D printed antenna prototype has size of 42.0 mm × 42.0 mm × 33.0 mm (including the waveguide flange) and a light weight of 14.1 g due to the low density (1.61 g/cm^3 at 25 °C) of the utilized resin.

IV. MEASUREMENT AND DISCUSSION

The reflection coefficient and radiation patterns of the fabricated antenna are measured with Keysight N5224A vector

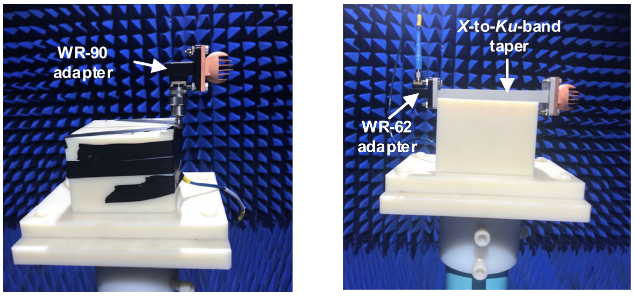

(a) (b)

FIGURE 11. **Photographs of the measurement setups in the anechoic chamber. (a) In the measurement at *X* band. (b) In the measurement at *Ku* band.**

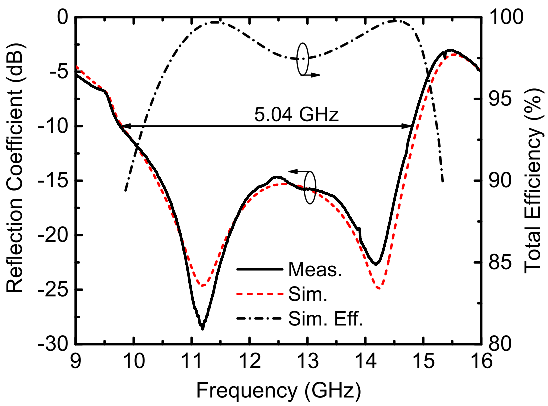

FIGURE 12. **Simulated and measured reflection coefficient (S_{11}) of the proposed antenna with its simulated radiation efficiency.**

network analyzer and an anechoic chamber, respectively. The RF performance at *X* and *Ku* bands was measured individually. In the measurement at *Ku* band, the antenna was mated to a WR62 waveguide-to-coax adapter through an *X*-to-*Ku* band waveguide taper. The measurement setups in the anechoic chamber is shown in Fig. 11.

The simulated and measured reflection coefficients are graphically compared in Fig. 12, showing excellent agreement that indicates high precision of the employed fabrication process. The result shows a wide operational bandwidth of the antenna from 9.77 to 14.81 GHz with a measured in-band reflection coefficient lower than -10 dB. This corresponds to a FBW of about 40.9%. The simulated in-band total efficiency of the antenna, as plotted in Fig. 12, is higher than 90%. The loss mainly comes from the roughness of the surface of the copper plating layer. The out-of-band total efficiency is much lower due to the degraded reflection coefficient. The practical efficiency is not obtained due to limitation of the chamber.

Fig. 13 shows the measured normalized radiation patterns, which also agree well with the simulated results. Apparently, directional radiation patterns are realized within the operational bandwidth. The measured cross polarization is mostly 15–20 dB lower than the measured co-polarization. The simulated and measured in-band realized gains of the antenna are

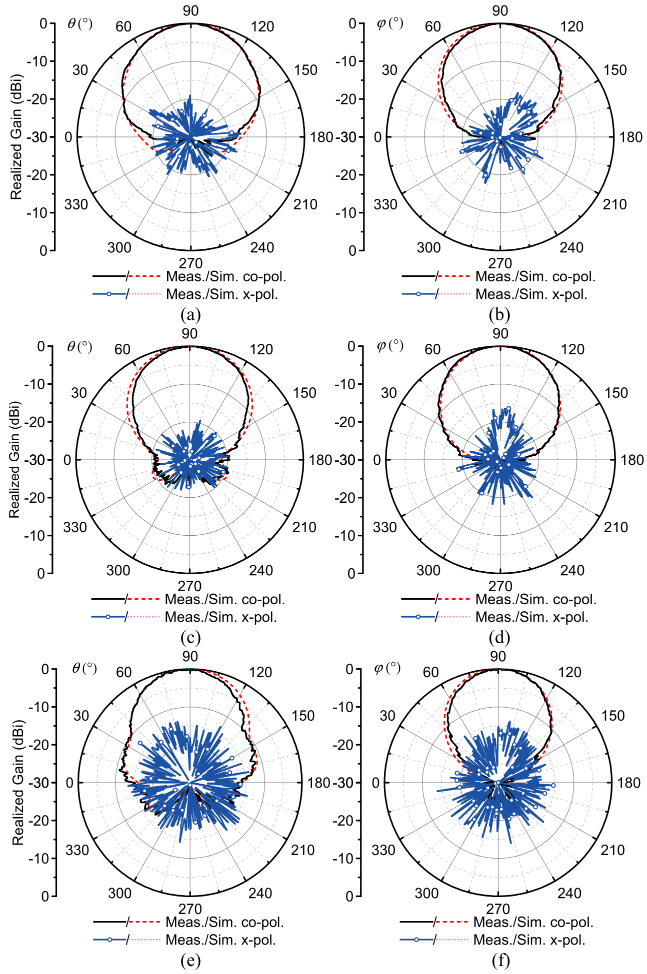

FIGURE 13. **Simulated and measured normalized radiation patterns of the proposed antenna.(a) *E*-plane at 10.7 GHz. (b) *H* -plane at 10.7 GHz. (c) *E*-plane at 12.2 GHz. (d) *H* -plane at 12.2 GHz. (e) *E* -plane at 14.8 GHz. (f) *H* -plane at 14.8 GHz.**

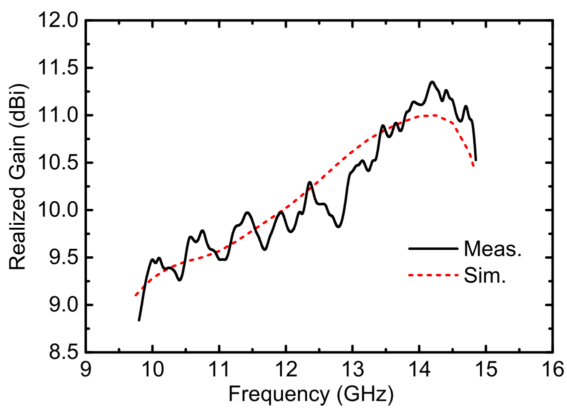

FIGURE 14. **Simulated and measured realized gain of the proposed antenna.**

shown in Fig. 14. The measured in-band realized gain is in a range of 8.8–11.3 dBi and agrees with the simulated values.

A quantitative comparison in major specifications of the demonstrated antenna with several waveguide slot antennas

TABLE 2. Comparison with previously reported works.

Ref.	Types	f (GHz)	FBW (%)	Gain (dBi)	R.C. (dB)	Fabrication Process
[2]	Unit	9.3	8.1	6.7	<-10	CNC
[3]	Unit	2.4	15	5.5	<-10	CNC
[6]	Array	10.1	14.9	18	<-15	CNC
[9]	Array	58.9	30	27.5	<-10	CNC
[10]	Unit	5.8	35.8	13.2	<-10	CNC
[11]	Unit	2	13	7	<-10	CNC
[19]	Array	15.1	12.6	26.3	<-10	3D printing
[20]	Array	15.1	12.9	32.5	<-14	3D printing
T.W.	Unit	12.3	40.9	11.2	<-10	3D printing

*T.W.: This work; f: Center frequency; R.C.: The measured in-band reflection coefficient.

and multi-mode antennas is summarized in Table 2. From it, it is apparent that the proposed antenna is featured as widest operation bandwidth with excellent radiation characteristic.

V. CONCLUSION

In this paper, a slot-loaded wideband spherical antenna under the operation of TM_{101} and TM_{211} modes is proposed, implemented and measured. By suitably etching some slots on the shell of a spherical resonator, two resonant modes (TM_{101} and TM_{211}) are excited and merged with each other, resulting in a wideband characteristic with two resonances. The antenna prototype operating at *X* and *Ku* bands is monolithically 3-D printed, featuring a light weight of 14.1 g, eliminated assembly tolerance, and simply fabrication process. The antenna demonstrates good directional radiation patterns in a wide FBW of 40.9% with an in-band realized gain of 8.8–11.3 dBi. Good agreement between the simulated and measured results indicates high precision of the utilized SLA printing and copper plating processes.

REFERENCES

[1] R. C. Hansen, *Phased Array Antennas*. New York, NY, USA: Wiley, 1998.

[2] S. Ebadi and K. Forooraghi, "An annular waveguide slot antenna," *IEEE Antennas Wireless Propag. Lett.*, vol. 6, pp. 525–528, 2007.

[3] K. W. Leung and L. Y. Chan, "The probe-fed zonal slot antenna cut onto a cylindrical conducting cavity," *IEEE Trans. Antennas Propag.*, vol. 53, no. 12, pp. 3949–3952, Dec. 2005.

[4] H. Zhao, R. Xu, and W. Wu, "Broadband waveguide slot array for SAR," *Electron. Lett.*, vol. 47, no. 2, p. 76, Jan. 2011.

[5] D. Kim and R. Elliott, "A design procedure for slot arrays fed by single-ridge waveguide," *IEEE Trans. Antennas Propag.*, vol. 36, no. 11, pp. 1531–1536, Nov. 1988.

[6] W. Wang, S.-S. Zhong, Y.-M. Zhang, and X.-L. Liang, "A broadband slotted ridge waveguide antenna array," *IEEE Trans. Antennas Propag.*, vol. 54, no. 8, pp. 2416–2420, Aug. 2006.

[7] Y. Miura, J. Hirokawa, M. Ando, Y. Shibuya, and G. Yoshida, "Double-layer full-corporate-feed hollow-waveguide slot array antenna in the 60-GHz band," *IEEE Trans. Antennas Propag.*, vol. 59, no. 8, pp. 2844–2851, Aug. 2011.

[8] H. Guan-Long, C. Tan-Huat, Z. Shi-Gang, and Y. Tat-Soon, "Broadband and high gain waveguide-fed slot antenna array in the Ku-band," *IET Microw., Antennas Propag.*, vol. 8, no. 13, pp. 1041–1046, Oct. 2014.

[9] A. Farahbakhsh, D. Zarifi, and A. U. Zaman, "A mmWave wideband slot array antenna based on ridge gap waveguide with 30% bandwidth," *IEEE Trans. Antennas Propag.*, vol. 66, no. 2, pp. 1008–1013, Feb. 2018.

[10] T. Chen, Y. Chen, and R. Jian, "A wideband differential-fed microstrip patch antenna based on radiation of three resonant modes," *Int. J. Antennas Propag.*, vol. 2019, pp. 1–7, Aug. 2019.

[11] N. Liu, L. Zhu, and W. Choi, "A differential-fed microstrip patch antenna with bandwidth enhancement under operation of TM_{10} and TM_{30} modes," *IEEE Trans. Antennas Propag.*, vol. 65, no. 4, pp. 1607–1614, Apr. 2017.

[12] X. Bi, G.-L. Huang, X. Zhang, and T. Yuan, "Design of wideband and high-gain slotline antenna using multi-mode radiator," *IEEE Access*, vol. 7, pp. 54252–54260, 2019.

[13] K. Zhang and D. Li, *Electromagnetic Theory for Microwaves and Optoelectronics*, 2nd ed. Berlin, Germany: Springer, 2008, pp. 235–314.

[14] K. Wa Leung, "Analysis of the zonal and rectangular slots on a conducting spherical cavity," *IEEE Trans. Antennas Propag.*, vol. 49, no. 12, pp. 1739–1745, Dec. 2001.

[15] K. Wa Leung, "Theory and experiment of a rectangular slot on a sphere," *IEEE Trans. Microw. Theory Techn.*, vol. 46, no. 12, pp. 2117–2123, May 1998.

[16] M. Plonus, "Electromagnetic scattering by slots on a sphere," *Proc. Inst. Elect. Eng.*, vol. 115, no. 5, p. 622, 1968.

[17] K. Wa Leung, "Rectangular and zonal slots on a sphere with a backing shell: Theory and experiment," *IEEE Trans. Antennas Propag.*, vol. 51, no. 7, pp. 1434–1442, Jul. 2003.

[18] Y. Mushiake and R. Webster, "Radiation characteristics with power gain for slots on a sphere," *IRE Trans. Antennas Propag.*, vol. 5, no. 1, pp. 47–55, Jan. 1957.

[19] G.-L. Huang, S.-G. Zhou, T.-H. Chio, and T.-S. Yeo, "Fabrication of a high-efficiency waveguide antenna array via direct metal laser sintering," *IEEE Antennas Wireless Propag. Lett.*, vol. 15, pp. 622–625, 2016.

[20] G.-L. Huang, S.-G. Zhou, and T.-H. Chio, "Highly-efficient self-compact monopulse antenna system with integrated comparator network for RF industrial applications," *IEEE Trans. Ind. Electron.*, vol. 64, no. 1, pp. 674–681, Jan. 2017.

[21] G. P. Le Sage, "3D printed waveguide slot array antennas," *IEEE Access*, vol. 4, pp. 1258–1265, 2016.

[22] C. Guo, X. Shang, M. J. Lancaster, and J. Xu, "A 3-D printed lightweight X-band waveguide filter based on spherical resonators," *IEEE Microw. Wireless Compon. Lett.*, vol. 25, no. 7, pp. 442–444, Jul. 2015.

[23] J. Li, C. Guo, L. Mao, J. Xiang, G.-L. Huang, and T. Yuan, "Monolithically 3-D printed hemispherical resonator waveguide filters with improved out-of-band rejections," *IEEE Access*, vol. 6, pp. 57030–57048, 2018.

[24] MathWorks, Inc., Natick, MA, USA, (Mar. 2018). *MATLAB*. [Online]. Available: http://www.mathworks.com

[25] ANSYS, Canonsburg, PA, USA. (Oct. 2018). *ANSYS High Frequency Structure Simulator*. [Online]. Available: https://www.ansys.com

[26] S. Silver, Ed., "Theory of slot radiators," *Microwave Antenna Theory and Design*. Stevenage, U.K.: Peregrinus.

[27] *3D CAD Design Software SOLIDWORKS*. Accessed: Oct. 2015. [Online]. Available: http://www.solidworks.com

[28] Somos. (May 2019). *Stereolithography Materials*. [Online]. Available: https://www.dsm.com

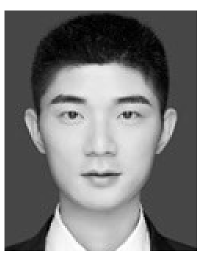

YU-JIAN ZHU was born in Zhoukou, China, in 1993. He received the B.E. degree in electronic information engineering from the Anyang Institute of Technology, Anyang, China, in 2016. He is currently pursuing the master's degree in information and communication engineering with Shenzhen University, Shenzhen, China. His current research interests include the patch antennas and waveguide slot antennas.

JIN LI (Member, IEEE) received the B.E. degree in electronic information engineering and the Ph.D. degree in radio physics from the University of Electronic Science and Technology of China, Chengdu, Sichuan, China, in 2010 and 2017, respectively.

From 2013 to 2015, he was a Visiting Research Scholar with the Birck Nanotechnology Center, School of Electrical and Computer Engineering, Purdue University, West Lafayette, IN, USA, supported by the China Scholarship Council under the State Scholarship Fund. From 2017 to 2018, he was an External Research Specialist with the ATR National Key Laboratory of Defense Technology, Shenzhen University, Shenzhen, Guangdong, China. He is currently a Postdoctoral Research Fellow with the College of Electronics and Information Engineering, Shenzhen University. His current research interests include RF design and characterization of reconfigurable microwave filters, microwave passive devices, RF microelectromechanical systems, thin film materials, and additively manufactured RF components.

Dr. Li is a member of the IEEE Microwave Theory and Techniques Society (IEEE MTT-S), the Chinese Institute of Electronics, and the Applied Computational Electromagnetics Society (ACES). He was a co-recipient of the First Place Award at the 2014 and 2015 IEEE MTT-S International Microwave Symposium Tunable RF-MEMS Filter Student Design Competitions. He is a Reviewer for several IEEE/IET/Wiley/ACES journals and international conferences.

XIAO ZHANG (Member, IEEE) was born in Gaozhou, China. He received the B.Eng. degree in information engineering and the M.Eng. degree in communication and information systems from the South China University of Technology, Guangzhou, China, in 2011 and 2014, respectively, and the Ph.D. degree in electrical and computer engineering from the University of Macau, Macau, in 2017.

From September 2012 to August 2014, he was a Research Assistant with Comba Telecom Systems Limited, Guangzhou, China. He joined the Antenna and Electromagnetic-Wave Laboratory, University of Macau, as a Research Fellow in January 2018. He is currently an Assistant Professor with the College of Information Engineering, Shenzhen University, Shenzhen, China. His research interests include planar antennas and microwave circuits.

TAO YUAN (Member, IEEE) received the B.E. degree in electronic engineering and the M.E. degree in signal and information processing from Xidian University, Xi'an, Shaanxi, China, in 1999 and 2003, respectively, and the Ph.D. degree in electrical and computer engineering from the National University of Singapore, Singapore, in 2009.

He is currently a Professor with the College of Electronics and Information Engineering, Shenzhen University, Shenzhen, Guangdong, China. His current research interest includes the development of novel RF modules and antennas for mobile terminals and 5G applications.

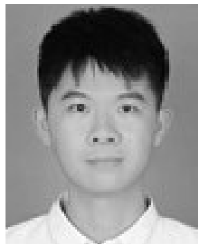

ZENG-PEI ZHONG received the B.E. degree in applied physics from Shenzhen University (SZU), Shenzhen, China, where he is currently pursuing the Ph.D. degree in information and communication engineering. His current research interests include circularly polarized antennas, navigation antennas, and antennas array.

TING-YAN TAN was born in Guigang, China, in 1996. She received the B.E. degree in electronic information engineering from Guangxi Normal University, Guilin, China, in 2018. She is currently pursuing the master's degree in information and communication engineering with Shenzhen University, Shenzhen, China. Her current research interests include the patch antennas and reconfigurable antennas.

XIAO-KUN BI was born in Henan, China, in 1987. He received the B.Sc. degree in electrical & information engineering from the North University of China, Taiyuan, China, in 2010, the M.Sc. degree in signal and information processing from Nankai University, Tianjin, China, in 2015, and the Ph.D. degree in electrical and computer engineering from the University of Macau, Macau, in 2019.

In 2014, he was a Research Assistant with the University of Macau. His research interests include notched-/dual-wideband bandpass filters, reconfigurable filters, slotline antennas, and their applications in modern communication systems.